Geometric Singular Perturbation Analysis of a Multiple Time-scale Model for Diabetes and COVID-19 Comorbidity

CHONTITA RATTANAKUL[1,2], YONGWIMON LENBURY[1,2],
NATHNARONG KHAJOHNSAKSUMETH[1,2], CHARIN MODCHANG[3,4]
[1] Department of Mathematics, Faculty of Science, Mahidol University, Rama 6 Rd., THAILAND
[2] Centre of Excellence in Mathematics, MHESI, Bangkok 10400, THAILAND
[3] Department of Physics, Faculty of Science, Mahidol University, Rama 6 Rd., THAILAND
[4] Centre of Excellence in Physics, MHESI, Bangkok 10400, THAILAND

Abstract: More and more information on mortality and morbidity indicates that in order to fight the COVID-19 pandemic, it is important to focus our attention on comorbidities. Several reports evidence of how many elderly patients who become severely ill exhibit underlying illness such as cardiovascular disease, kidney disease, tumor, and more to our special attention here, type 2 diabetes. Better understanding of the mechanism underlying the comorbidity between different diseases requires merging models of systems across different time-scales. The model homogenization across multiple spatial and time scales poses an important challenge to researchers in the field of medical science. An approach that has been found relatively efficient in the analysis of such models is the use of singular perturbation technique. Here, we study a differential equation model system with multiple time scales which describes the diabetes and COVID-19 comorbidity. It tracks the changes in levels of plasma glucose, insulin, and functional-cells, incorporating insulin resistance and inflammation responses. The model is analyzed with the geometric singular perturbation technique, by which conditions on the system parameters may be derived to identify regions in which the system exhibits different dynamic behavior, whether the system would be stable, or eventually oscillate in a sustained fashion. Discussion of these conditions allows us to better understand how comorbidity mediates the development of life-threatening symptoms in a diabetic patient in order that proper care and treatment may be prescribed.

Key-Words: Diabetes model, COVID-19, comorbidity, geometric singular perturbation analysis

Received: March 31, 2022. Revised: July 4, 2022. Accepted: August 22, 2022. Published: September 5, 2022.

1 Introduction

The spread of coronavirus across the globe has developed into a major pandemic which impacts all aspects of the human society. A great deal of research effort has been devoted to modeling and prediction of the progress of coronavirus infection and its impacts of social distancing and other measures in various countries hit hard by the pandemic, for example in [1], [2] and [3].

According to Smith [4], medical doctors have been investigating an unexpected coronavirus complication that can appear a couple of weeks or sometimes months, after the initial COVID-19 infection. Increasing number of patients have been reported to develop life-threatening symptoms that necessitate prompt medical attention. This new complication of corona virus is dangerous and persists throughout a patient's life since, although both type 1 and type 2 diabetes can be managed with treatment, diabetes can't be cured, which means some patients will need expensive insulin therapy for the rest of their lives [4]. Although most patients will survive COVID infection, many of them experience long-term symptoms that frequently require medical attention. Moreover, quite a few even progress to multisystem inflammatory syndrome, according to Smith[4].

According to Campbell[5], patients with type 1 diabetes are more likely to die of Covid-19 than those with type 2. Also, NHS research confirmed that diabetes in coronavirus patients significantly increases the risk of their dying. "Almost one in three of all deaths from coronavirus among people in hospitals in England during the pandemic have been associated with diabetes," according to the study[5].

In an attempt to gain a better understanding of such complication, we consider here a model system of differential equations that describes the glucose-insulin dynamics, based on that proposed by De Gaetano et al. [6] and those mentioned in the work on the computational patient having diabetes and COVID by Barbiero and Lió[7], incorporating the effects of inflammatory response and insulin resistance, which we have modified to take into account the drastically different time scales observed in the time variations

of the concentrations of glucose, insulin, the number of functional β-cells and the inflammatory response.

The presence of glucose (glycaemia) and insulin in one's blood is regulated through a negative feedback loop in which plasma glucose stimulates β-cells to release insulin giving rise to insulin-mediated increase in tissue glucose uptake while liver gluconeogenesis and glycogenolysis are decreased [6].

In 2001, a nonlinear mathematical model of the glucose-insulin control mechanism was proposed by Lenbury et al.[8], taking into account the role of β-cells in maintaining and regulating insulin level in human's bloodstream. They utilized a gastrointestinal term to model the absorption of glucose by the intestine, and the entry of glucose into the human's plasma, under the assumption that this process declines exponentially with time. The model is analyzed using the geometric singular perturbation method by which various conditions on the system parameters are obtained to identify different dynamic behavior exhibited by the system, including the possibility of limit cycle behavior in the system model which closely simulates sustained oscillatory time series often observed in experimental data. To take into account the temporal absorption of glucose, they used a sinusoidal term with the means to study how the patients respond when subject to ambulatory-fed conditions. The resulting model equations are as follows.

$$\begin{aligned}
\frac{dx}{dt} &= r_1 zy - r_2 zx + c_1 z \\
\frac{dy}{dt} &= \frac{R_3 N}{z} - R_4 x + C_2 + w(t) \\
\frac{dz}{dt} &= R_5(y - \hat{y})(T - z) + R_6 z(T - z) - R_7 z
\end{aligned}$$

where x and y are the differences in the plasma insulin and glucose concentrations from their respective fasting (basal) concentrations, and z represents the density of the pancreatic β-cells in the proliferative phase.

In 2008, Giang et al.[9] analyzed a delay model of the glucose-insulin system proposed by Palumbo et al. in [10]. They proved persistence, as well as existence and stability of a unique positive equilibrium point of the model system. Moreover, their work [9] illustrates uniform persistence and global stability of equilibrium solutions. Using omega limit set of a persistent solution and the full time solution that they derived, they were able to investigate the effect of delays in terms of oscillating solutions. In addition, global stability and slowly oscillating behavior were shown to be possible provided suitable conditions on the system parameters are satisfied. The model equations under consideration are as follows.

$$\begin{aligned}
\dot{G}(t) &= -K_{xg} G(t) - K_{xgi} G(t) I(t - \tau_i) + \frac{T_{gh}}{V_G} \\
\dot{I}(t) &= -K_{xi} I(t) + \frac{T_{iG_{max}}}{V_I} f(G(t - \tau_g))
\end{aligned}$$

where $f(G) = \dfrac{G^\gamma}{G^\gamma + G_*^\gamma}$ with $\sup\limits_{G \geq 0} f(G) = 1$, G and I are, respectively, glucose and insulin concentrations, with corresponding delays of τ_g and τ_i.

In the same year, Kardar et al.[11] made use of an advisory/control algorithm in aide of out-patients suffering from insulin dependent diabetes mellitus. Utilizing Mamdani type fuzzy logic controllers, their advisory/control algorithm combines expert knowledge about diabetes treatments in the attempt to regulate the glucose level in bloodstream, while the patient is experiencing disturbances in glucose concentration due to food intakes or there are fluctuations in the measured plasma glucose level due to measurement errors.

Also in 2008, De Gaetano et al.[6] studied a model of the pancreatic islet compensation, and identified certain basic qualitative characteristics of the model's solutions. They simulated the model's performance over one's lifetime under different conditions. They then compared their model with two previous models of diabetes progression, and concluded that the proposed model provided a realistic and robust description of the glucose-insulin process in healthy and diabetic person. More importantly, by varying the size of one of the system parameters, their model can be reduced to either "fast", providing short-term prediction, or "slow" subsystems, which describes long-term progression.

In 2015, Cao et al.[13] studied a model which consists of four states of type 2 diabetes, assuming no input or output. Using a model consisting of partial differential equations, a general well-posedness result was obtained and the exponential stability of dynamic solution was shown. The steady-state solution predicts the diabetics' stable distribution probability[13].

The models mentioned above are useful in answering a number of crucial questions concerning the progression of diabetes mellitus. However, in the model analyses, they did not take into account the fact that the state variables under consideration vary with time at extremely different time scales.

Moreover, we observe that the model of De Gaetano et al.[6] has not properly accounted for the reports that the ability of the cells to absorb or use up blood sugar appears to decline as the glucose concentration in the bloodstream increases to a high level. It is mentioned in [14], that in a patient with predi-

abetes conditions, the pancreas has to work harder to release sufficient amount of insulin in order to control the glucose in the bloodstream to a satisfactory low level. It is well-known that insulin resistance takes place when too much glucose in the blood decreases the cells' ability to absorb and use blood sugar for energy [14]. We will therefore introduce a term in our model, which is based on that in [6], to take into account the reduction in the ability of cells to control plasma glucose when its concentration becomes too high. For a patient with prediabetes conditions, we express the insulin resistance term as a function of glucose concentration, so that it rises as the glucose level increases.

Recently, Ratanakul et al.[15] attempted to incorporate this insulin resistance effect more explicitly, as well as account for the diversified time scales in their model, which was analyzed by the geometric singular perturbation method, upon assuming that the level of β-cells remains relatively constant and thus reducing the model analysis into a 2-dimensional singular perturbation argument. In our present work, the functional β cells is tracked, and although it is considered to vary slowly, it is not taken to be constant in our analysis, making it necessary to carry out the geometric singular perturbation analysis in the 3-dimensional space.

To account for comorbidity between diabetes and COVID-19, an equation describing the rate of change in the inflammatory response is added to the model, following that given in the work by Barbiero and Lió [7]. In this equation, the rate of change of inflammatory response is taken to depend on abnormal ACE2 activity, SARS-CoV-2 affinity with ACE2, the re-enforcement of inflammation due to drug surplus left inside the body, inflammation rate due to glucose surplus, and the anti-inflammatory response rate as suggested in [7]

We will explain in subsequent sections that, based on values of our model system parameters, reported in various literature, we may conclude that the level of plasma glucose varies relatively quickly, whereas the number of β-cells changes at a much larger time scale, and insulin concentration, on the other hand, can be said to change at an intermediate speed relatively. We shall then use two small parameters to merge such diversified time-scales. Arguments based on singular perturbation theory is thus the appropriate geometric method of analysis which is applied to identify different dynamic behavior permitted by our model.

2 Materials and Methods

Insulin, $I(t)$, is a chemical messenger produced in one part of the body to have an action on another. It is a protein responsible for regulating blood glucose levels, $G(t)$, as part of the metabolism. The control of blood sugar, or glucose, by insulin is a negative feedback mechanism. When blood sugar rises, from our food intake for example, receptors in the body sense a change. In response, the control center, namely the pancreas, is stimulated. In the pancreas, the functional beta cells, $\beta_f(t)$, are designed to function as "fuel sensors" triggered by glucose[16]. As glucose levels rise in the plasma of the blood, uptake and metabolism by the pancreas beta cells are enhanced, leading to insulin secretion into the bloodstream which has the effect of lowering plasma glucose levels. Once blood sugar levels reach a state of equilibrium (homeostasis), the pancreas stops releasing insulin.

Thus, the drop in the rate of increase of plasma glucose sends a negative feed-back to signal the functional beta cells in the pancreas to reduce the production of insulin. In this way, the glucose-insulin control system in a healthy human's body functions has a negative feed-back loop that regulates the glucose level in the blood stream.

We are thus led to the following model system of differential equations, which has been adapted from [6],[7], and [15].

$$\frac{dG}{dt} = R_0 - E_{G0}G - S_I\frac{GI}{I_{RS}+i}, \quad G(t_0) = G_0 \tag{1}$$

$$\frac{dI}{dt} = \sigma\frac{\beta_f G^{\nu_h}}{\alpha + G^{\nu_h}} - kI, \quad I(t_0) = I_0 \tag{2}$$

$$\frac{d\beta_f}{dt} = -r_0 + r_1 G - r_2 G^2\beta_f, \quad \beta_f(t_0) = \beta_{f0} \tag{3}$$

$$\frac{dI_{RP}}{dt} = k_{SARS}\Delta k_{ACE2,0} + k_D D_s + k_G G - k_{eff} I_{RP}, \quad I_{RP}(t_0) = I_{PR0} \tag{4}$$

The insulin resistance term I_{RS} , in the denominator of the last term in (1), is expressed as the following function of glucose concentration:

$$I_{RS} = a_0 G^2 + b_0 G + c_0 \tag{5}$$

following the observation mentioned earlier that insulin resistance occurs when excess glucose in the blood reduces the ability of the cells to absorb and use blood sugar for energy [15], so that the ability of cells to control plasma glucose declines when glucose concentration becomes too high. Here, a_0 is the second order coefficient for insulin resistance, b_0 is the first order coefficient for insulin resistance, and c_0 is insulin resistance at zero glucose.

Table 1: State variables and parameters appearing in the model equations (1) - (5) with their descriptions

Item	Description	Unit
G	glucose concentration in bloodstream	G^*
I	insulin concentration in bloodstream	I^*
β_f	density of functional β cells	β_f^*
I_{RS}	insulin resistance	I_{RS}^*
I_{RP}	inflammatory response	I_{RP}^*
t	time	t^*
R_0	rate of glucose production at zero glucose	$G^*(t^*)^{-1}$
S_I	insulin sensitivity	$I_{RS}^*(t^*I^*)^{-1}$
E_{G0}	specific rate of glucose removal at zero insulin	$(t^*)^{-1}$
i	insulin resistance self-inhibition coefficient	I_{RS}^*
μ	$i + c_0$, c_0 being insulin resistance at zero glucose	I_{RP}^*
σ	maximal rate of insulin secretion by β cells	$I^*(\beta_f^* t^*)^{-1}$
α	glucose concentration yielding 50% of insulin secretion	$(G^*)^{\nu_h}$
k	combined specific rate of , insulin uptake at the liver kidneys, and insulin receptors	$(t^*)^{-1}$
ν_h	power coefficient for Hill-shaped glycemia effect on pancreatic insulin release, set to 4 as done in [6]	None
r_0	death rate of functional β cells at zero glucose	$\beta_f^*(t^*)^{-1}$
r_1	I-order coefficient for β cell replication	$\beta_f^*(G^*t^*)^{-1}$
r_2	II-order coefficient for β cell replication	$(G^*)^{-2}(t^*)^{-1}$
k_{SARS}	inflammation rate due to SARS-CoV-2	$I_{RP}^*\left(k_{ACE2}^* t^*\right)^{-1}$
$k_{ACE2,0}$	normal ACE-catalyzed conversion rate	k_{ACE2}^*
Δ	multiple of normal conversion rate	None
k_D	specific inflammation rate due to ACEi surplus	$I_{RP}^*\left(D_r^* t^*\right)^{-1}$
D_s	surplus drug concentration	D_s^*
k_G	specific inflammation rate due to glucose surplus	$I_{RP}^*(G^*t^*)^{-1}$
k_{eff}	specific anti-inflammatory response rate	$(t^*)^{-1}$
a_0	II-order coefficient for insulin resistance	$I_{RS}^*(G^*)^{-2}$
b_0	I-order coefficient for insulin resistance	$I_{RS}^*(G^*)^{-1}$
c_0	insulin resistance at zero glucose	I_{RS}^*

The variables and parameters appearing in (1)-(5) and their definitions are summarized in Table 1. The unit of each of the variables or parameters is denoted here as the star,$(\cdot)^*$, of the corresponding quantity $(\cdot)$, as it depends on the choice of units used by a particular researcher to measure these quantities.

In Equation (1) for the rate of change of glucose concentration, following that given in [15], the first term on the right, R_0 , is the rate of glucose production at zero glucose. The last term is the inhibition on the rise of glucose exerted by the secretion of insulin, where E_{G0} is the specific rate of glucose removal at zero insulin, and S_I represents the normal insulin sensitivity [7].

In Equation (2), the same as that used in [7] and by De Gaetano et al. [6], the first term on the right accounts for the increase in insulin level due to the increasing level of glucose, with σ being the maximal rate of secretion of insulin by β-cells, and α the glucose concentration yielding 50% of insulin secretion. Here, ν_h is the power coefficient for the Hill-shaped glycemia effect on pancreatic insulin release. This is set to 4 in [6]. The last term here is the rate of removal of insulin by natural means depending on how much insulin is present, with k being the removal rate constant of variation.

Equation (3) describes the rate of change of functional β-cells, following [7], where r_0 is the death rate of β-cells at zero glucose, r_1 the first order coefficient for β-cells replication, and r_2 is the second order coefficient for β-cells replication [7].

Equation (4) has been modified from that mentioned in [7]. The rate of increase of inflammatory response I_{RP} is taken to vary, in the absence of drug residuals, glucose or insulin, as a product of inflammation factor due to SARS-CoV-2 infectivity, with k_{SARS} representing the SARS-CoV-2 affinity with ACE2, and the abnormal activity of ACE2, $\Delta k_{ACE2,0}$, which we express here as a multiple Δ of the normal value $k_{ACE2,0}$ of k_{ACE2} . According to [17], for someone who has diabetes, taking an ACE inhibitor or ARB can help to control high blood pressure which increases the risk of problems from diabetes. Diabetes can damage the blood vessels in the kidneys, and high blood pressure can also damage the kidneys. According to [7], ACE inhibitor or ARB treatments could increase ACE2 abundance and thus enhance viral entry. The second term on the right of (4) therefore accounts for the increase in inflammatory response due to drug that remains in the patient's body, k_D being the rate constant in the inflammation rate due to ACE inhibitor surplus. Assuming continual treatments by ACE inhibitor, the quantity D_S in (4) is set to the mean value of 0.0372 mg/ml on day 29 of Sotrovimab treatment, as given in [18].

The third term in (4) is the inflammation rate due

to glucose surplus, with k_G being the rate constant for this mechanism. Finally, the last term in (4) accounts for the anti-inflammatory response, which varies directly as the inflammation response at time t, with constant of variation k_{eff}.

Before we carry out the singular perturbation analysis, we need the following result concerning the invariance property of the model system. To that end, we let

$$\bar{G} = \frac{R_0}{E_{G0}}, \quad \underline{G} = \frac{\bar{k_1}}{E_{G0}}, \quad \bar{I} = \frac{\sigma}{k}, \tag{6}$$

$$\bar{\beta_f} = \frac{\bar{k_2}}{r_2 \underline{G}^2}, \quad \bar{I}_{RP} = \frac{\bar{k_3}}{k_{eff}}, \tag{7}$$

$$\bar{k_1} = R_0 - S_I \frac{\bar{I}}{b_0}, \quad \bar{k_2} = -r_0 + r_1 \bar{G}, \tag{8}$$

$$\bar{k_3} = k_{SARS} \Delta k_{ACE2,0} + k_D D_S + k_G \bar{G} \tag{9}$$

Lemma 2
Noting that all model parameters are positive, we let $\mathcal{B}$ be the set in the $\big(G, I, \beta_f, I_{RP}\big)$-space defined as

$$\begin{aligned}\mathcal{B} = \{ \big(G, I, \beta_f, I_{RP}\big) \in \mathbb{R}^4 : \underline{G} \le G \le \bar{G}, \\ 0 < I \le \bar{I}, 0 < \beta_f \le \bar{\beta}_f, 0 < I_{RP} \le \bar{I}_{RP} \}\end{aligned} \tag{10}$$

Then, $\mathcal{B}$ is positive invariant and all solutions starting in $\mathcal{B}$ are uniformly bounded, provided

$$\min\{\bar{k_1}, \bar{k_2}\} > 0 \tag{11}$$

Proof
Suppose $\big(G_0, I_0, \beta_{f0}, I_{RP0}\big) \in \mathcal{B}$. First, we show that G, I, β_f, and I_{RP} remain positive.

By contradiction, if G were to be negative at some point in $\mathcal{B}$, then there has to be a $t_0 > 0$ where $G(t_0) = 0$ and $G'(t_0) < 0$. However, by (1), at this point,

$$\begin{aligned}\left.\frac{dG}{dt}\right|_{t=t_0} &= R_0 - E_{G0} G(t_0) - S_I \frac{G(t_0) I(t_0)}{I_{RS}(t_0) + i} \\ &= R_0 > 0\end{aligned}$$

which is a contradiction, and thus G never vanishes.

Similarly, if I were to be negative at some point in $\mathcal{B}$, then there has to be a $t_0 > 0$ where $I(t_0) = 0$ and $I'(t_0) < 0$. However, by (2), at this point,

$$\begin{aligned}\left.\frac{dI}{dt}\right|_{t=t_0} &= \sigma \frac{\beta_f G^{\nu_h}(t_0)}{\alpha + G^{\nu_h}} - k I(t_0) \\ &= \sigma \frac{\beta_f G^{\nu_h}(t_0)}{\alpha + G^{\nu_h}} > 0\end{aligned} \tag{12}$$

since we have already shown that G is always positive. This is a contradiction, and thus I never vanishes.

Next, if β_f were to be negative at some point in $\mathcal{B}$, then there has to be a $t_0 > 0$ where $\beta_f(t_0) = 0$ and $\beta_f'(t_0) < 0$. However, by (3), at this point

$$\begin{aligned}\left.\frac{d\beta_f}{dt}\right|_{t=t_0} &= -r_0 + r_1 G(t_0) - r_2 G^2(t_0) \beta_f(t_0) \\ &= -r_0 + r_1 G(t_0) \\ &> -r_0 + r_1 \underline{G} \quad > 0\end{aligned}$$

due to (11). This is a contradiction, and thus β_f never vanishes.

Finally, if I_{RP} were to be negative at some point in $\mathcal{B}$, then there has to be a $t_0 > 0$ where $I_{RP}(t_0) = 0$ and $I_{RP}'(t_0) < 0$. However, by (4), at this point,

$$\begin{aligned}\left.\frac{dI_{RP}}{dt}\right|_{t=t_0} &= k_{SARS} \Delta k_{ACE2,0} + k_D D_S + k_G G(t_0) \\ &\quad - k_{eff} I_{RP}(t_0) \\ &> k_{SARS} \Delta k_{ACE2,0} + k_D D_s > 0\end{aligned}$$

which, again, is a contradiction, and thus I_{RP} never vanishes.

Now, we consider the system (1)-(4) with $\big(G_0, I_0, \beta_{f0}, I_{RP0}\big) \in \mathcal{B}$, and first show that I is bounded. From (2), we have

$$\frac{dI}{dt} = \sigma \frac{\beta_f G^{\nu_h}}{\alpha + G^{\nu_h}} - kI \le \sigma \bar{\beta}_f - kI$$

Then, by the comparison theorem, one has

$$I \le I_0 e^{-kt} + \frac{\sigma}{k}\big(1 - e^{-kt}\big) \le \bar{I} e^{-kt} + \bar{I}\big(1 - e^{-kt}\big) = \bar{I}$$

using (6). Thus, I remains bounded above by $\bar{I}$. Then, from (1), we have

$$\frac{dG}{dt} = R_0 - E_{G0} G - S_I \frac{GI}{I_{RS} + i} \le R_0 - E_{G0} G$$

Thus, by the comparison theorem, we have

$$\begin{aligned}G &\le G_0 e^{-E_{G0} t} + \frac{R_0}{E_{G0}}\big(1 - e^{-E_{G0} t}\big) \\ &\le \bar{G} e^{-E_{G0} t} + \bar{G}\big(1 - e^{-E_{G0} t}\big) = \bar{G}\end{aligned}$$

using (6). Therefore, G remains bounded above by $\bar{G}$. On the other hand, (1) gives

$$\frac{dG}{dt} \ge R_0 - E_{G0} G - S_I \frac{\bar{I}}{b_0} = \bar{k}_1 - E_{G0} G$$

Thus, by the comparison theorem, we have

$$\begin{aligned}G &\ge G_0 e^{-E_{G0} t} + \frac{\bar{k}_1}{E_{G0}}\big(1 - e^{-E_{G0} t}\big) \\ &\ge \underline{G} e^{-E_{G0} t} + \underline{G}\big(1 - e^{-E_{G0} t}\big) = \underline{G}\end{aligned} \tag{13}$$

using (6) and (11). Therefore, G remains bounded

below by $\underline{G}$. From (3),
$\frac{d\beta_f}{dt} \leq -r_0 + r_1\bar{G} - r_2\underline{G}^2\beta_f = \bar{k}_2 - r_2\underline{G}^2\beta_f$
using (9). Then, by the comparison theorem, we have

$$\begin{aligned}\beta_f &\leq \beta_{f0}e^{-r_2\underline{G}^2 t} + \frac{\bar{k}_2}{r_2\underline{G}^2}\big(1 - e^{-r_2\underline{G}^2 t}\big) \\ &\leq \bar{\beta}_f e^{-\frac{r_0 r_2}{r_1}t} + \bar{\beta}_f\big(1 - e^{-\frac{r_0 r_2}{r_1}t}\big) = \bar{\beta}_f \qquad (14)\end{aligned}$$

using (7). Thus β_f remains bounded above by $\bar{\beta}_f$. Finally, (4) gives

$$\begin{aligned}\frac{dI_{RP}}{dt} &\leq k_{SARS}\Delta k_{ACE2,0} + k_D D_S + k_G\bar{G} - k_{eff}I_{RP} \\ &\leq \bar{k}_3 - k_{eff}I_{RP}\end{aligned}$$

using (9) and (11). Then, by the comparison theory, we have

$$\begin{aligned}I_{RP} &\leq I_{RP0}e^{-k_{eff}t} + \frac{\bar{k}_3}{k_{eff}}\big(1 - e^{-k_{eff}t}\big) \\ &\leq \bar{I}_{RP}e^{-kt} + \bar{I}_{RP}\big(1 - e^{-kt}\big) = \bar{I}_{RP}\end{aligned}$$

using (7). Thus, I_{RP} remains bounded above by $\bar{I}_{RP}$.

Hence, we have shown that $\mathcal{B}$ is positive invariant, and all solutions starting in $\mathcal{B}$ remain uniformly bounded. □.

With the above result, we are in the position to analyze the model to identify various dynamic behavior permitted by the system. Substituting (5) into (1), we introduce the following change of variables and parameters, to scale out their units, and to reflect, with the use of small scaling factors ε and δ , the observation mentioned earlier that G appears to be varying at a very fast speed. β_f varies at an extremely slow speed, whereas I varies at an intermediate speed, relatively, with time. As for I_{RP} , we see in [7] that k_{eff} is noticeable larger than k_D or k_G, it is reasonable to assume that I_{RP} varies at more or less the same speed as I. Letting

$$G' = \frac{G}{G^*}, I' = \frac{I}{I^*}, \beta'_f = \frac{\beta_f}{\beta_f^*}, I'_{RS} = \frac{I_{RS}}{I^*_{RS}}, \quad (15)$$

$$I'_{RP} = \frac{I_{RP}}{I^*_{RP}}, R'_0 = \frac{R_0 t^*}{G^*}, E'_{G0} = E_{G0}t^*, \quad (16)$$

$$S'_I = \frac{S_I I^* t^*}{a_0(G^*)^2}, b'_0 = \frac{a_0 b_0}{G^*}, \mu = \frac{a_0(c_0 + i)}{(G^*)^2}, \quad (17)$$

$$\sigma' = \frac{\sigma t^* \beta_f^*}{\varepsilon I^*}, \alpha' = \frac{\alpha}{(G^*)^{\nu_h}}, k' = \frac{kt^*}{\varepsilon}, \quad (18)$$

$$r'_0 = \frac{r_0 t^*}{\varepsilon\delta\beta_f^*}, r'_1 = \frac{r_1 G^* t^*}{\varepsilon\delta\beta_f^*}, r'_2 = \frac{r_2(G^*)^2 t^*}{\varepsilon\delta}, \quad (19)$$

$$k'_{ACE2} = \frac{k_{ACE2}}{k^*_{ACE2}}, k'_{SARS} = \frac{k^*_{SARS}k^*_{ACE2}t^*}{I^*_{RP}}, \quad (20)$$

$$D'_S = \frac{D_S}{D_S^*}, k'_D = \frac{k_D D_S^* t^*}{I^*_{RP}}, \quad (21)$$

$$k'_G = \frac{k_G G^* t^*}{I^*_{RP}}, k'_{eff} = k_{eff}t^* \quad (22)$$

where $(\cdot)^*$ denotes the unit of the corresponding quantity $(\cdot)$, and substituting the above new variables and parameters into (1) - (4), then dropping the primes, we arrive at the following model system, equivalent to (1) - (4).

$$\begin{aligned}\frac{dG}{dt} &= R_0 - G\left(E_{G0} + S_I\frac{I}{G^2 + b_0 G + \mu}\right) \\ &\equiv f(G, I) \qquad (23)\end{aligned}$$

$$\begin{aligned}\frac{dI}{dt} &= \varepsilon\left(\sigma\frac{\beta_f G^{\nu_h}}{\alpha + G^{\nu_h}} - kI\right) \\ &\equiv g(G, I, \beta_f) \qquad (24)\end{aligned}$$

$$\begin{aligned}\frac{d\beta_f}{dt} &= \varepsilon\delta\Big(-r_0 + r_1 G - r_2 G^2\beta_f\Big) \\ &\equiv h(G, \beta_f) \qquad (25)\end{aligned}$$

$$\frac{dI_{RP}}{dt} = k_{SARS}\Delta k_{ACE2} + k_D D_S + k_G G - k_{eff}I_{RP} \quad (26)$$

where now the variables are dimensionless, since we have scaled out their corresponding units. Their orders of magnitude depend on our choice of the units, $G^*, I^*, \ldots$ and so on. However, their rates of change are of different orders of magnitude, due to the small sizes of ε and δ , as well as the sizes of the parameters appearing in the equations.

We see that, once G is known by solving (23)-(25), I_{RP} can be found by solving (26), which does not affect Equations (23)-(25) in any way, we can essentially leave (26) out of the singular perturbation arguments for the time being and concentrate on the system of 3 equations (23)-(25) which are now in the appropriate form on which geometric singular perturbation analysis can be applied in the next section.

3 Model Analysis

3.1 Equilibrium Manifolds

Considering (23) - (25), we see that when f, g, and h are finite and nonzero, $\left|\frac{dG}{dt}\right| = O(1), \left|\frac{dI}{dt}\right| = O(\varepsilon)$, and $\left|\frac{d\beta_f}{dt}\right| = O(\varepsilon\delta)$, so that, for small ε and δ , G,

the scaled glucose concentration, has the fastest dynamics, while I, the scaled insulin concentration, has intermediate dynamics, and β_f the scaled functional β -cells density, varies at the slowest speed amongst the three state variables. Then, for sufficiently small values of ε and δ, under suitable regularity conditions, the singular perturbation theory allows approximating the solution of the system (23) - (25) with a sequence of simple dynamic transitions occurring at different speeds. More specifically, for sufficiently small ε and δ, the solution of the model system will stay within a θ-tube around the approximating transitions for some small θ , $\theta > 0$, which approaches 0 as ε and δ tend to zero. For more detailed description of the singular perturbation theory and the geometric perturbation technique, please see [19, 20]. This method of analysis allows us to predict how the solution trajectories will appear when the model's state variables are changing at radically heterogenous time scales. Without using this method, many dynamic behavior may be hidden and cannot be identified. In addition, the delineating conditions that allow such dynamics may not possibly be derived explicitly. If the state variables were treated as having the same dynamics, then we may miss the solution trajectories that could be observed only if one variable were recognized to have a very slow dynamics in comparison with the other state variables. Specifically, supported by the values of the physiological parameters reported in the literature [6] and [7], the functional beta cells have been found to possess a very slow dynamics since the size of its derivative is of order $\varepsilon\delta$, while glucose has a fast dynamics since its derivative is $O(1)$. Insulin, on the other hand, has the intermediate dynamics, its rate of change is of the order ε, where ε and δ are small and < 1.

To analyze the model, we first identify and describe the 3 equilibrium manifolds of interest.

The slow equilibrium manifold

The slow equilibrium manifold is obtained by equating the right hand side of (25) to zero. Solving it for β_f in terms of G, we arrive at the following equation.

We observe that, on this manifold, $\beta_f = 0$ when

$$G = G_* \equiv \frac{r_0}{r_1} \tag{27}$$

and $\beta_f < 0$ if G becomes smaller than G_* . Moreover, $\beta_f \to 0$ as $G \to \infty$, and $\beta_f \to -\infty$, as $G \to 0$. We can easily find that, on this surface,

$$\frac{d\beta_f}{dG} = \frac{\left(-r_1 G + 2r_0\right)}{r_2 G}$$

which means the slope of the graph will become 0 when

$$G = \frac{2r_0}{r_1} \equiv \hat{G} = 2G_*$$

$$\beta_f = \frac{r_1 G - r_0}{r_2 G^2} \tag{28}$$

Thus, the graph of this surface, for appropriate parametric values, may be depicted as in Fig.1a)

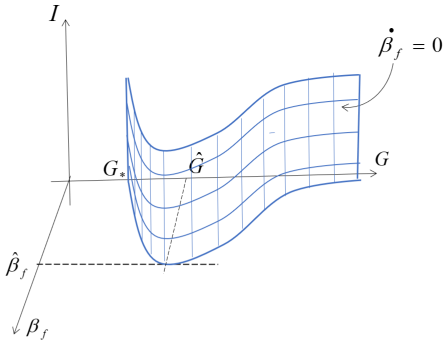

a)

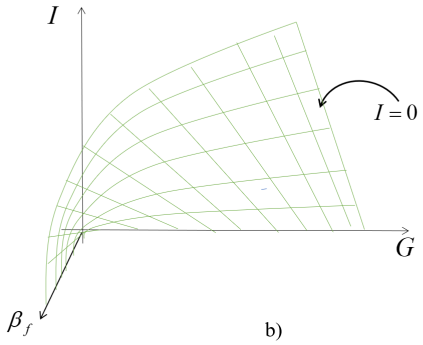

b)

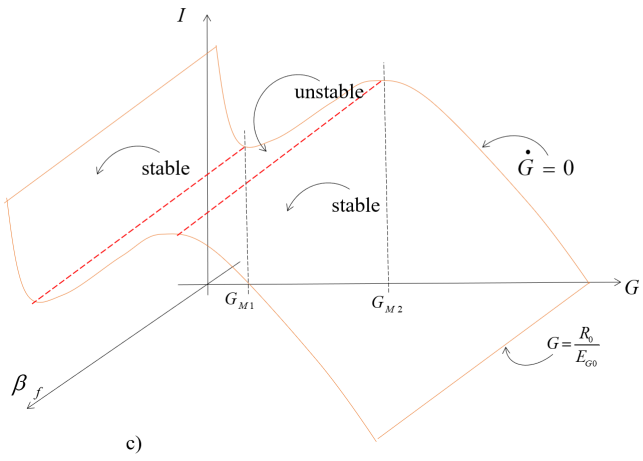

c)

Figure 1: The equilibrium manifolds: a) the slow manifold, b) the intermediate manifold, c) the fast manifold.

By considering (25), we know that when we are in the front of the surface where β_f is large, here $\frac{d\beta_f}{dt} < 0$, then the transition will take us in the direction of decreasing β_f until the surface $\frac{d\beta_f}{dt} = 0$ is reached. On the other hand, if we start at the point behind this surface where β_f is small, then $\frac{d\beta_f}{dt} > 0$ there and the transition will take us in the direction of increasing β_f until the surface $\frac{d\beta_f}{dt} = 0$ is reached. These transitions will be very slow since $\left|\frac{d\beta_f}{dt}\right| = O(\varepsilon\delta)$.

The intermediate equilibrium manifold

The intermediate equilibrium manifold is obtained by equating the right hand side of (24) to zero. Solving the resulting equation for I in terms of G, we arrive at the following equation.

$$I = \frac{\sigma\beta_f G^{\nu_h}}{k\alpha + kG^{\nu_h}} \tag{29}$$

We observe that, on this manifold, $I \to \frac{\sigma\beta_f}{k}$ as $G \to \infty$, and $I \to 0$ as $G \to 0$ when β_f is constant. On the other hand, when G is kept constant,$I \to \infty$ as $\beta_f \to \infty$, and $I \to 0$ as $\beta_f \to 0$. The graph of this surface, for appropriate parametric values, may be depicted as in Fig.1b) Looking at (24), we see that when we are above this surface where I is large, $\frac{dI}{dt} < 0$ here, and then the transition will take us in the direction of decreasing I until the surface is reached where $\frac{dI}{dt} = 0$. On the other hand, if we start at the point below this surface where I is small, then $\frac{dI}{dt} > 0$ there and the transition will take us in the direction of increasing I until the surface $\frac{dI}{dt} = 0$ is reached at which point the transition stops. These transitions will be made at an intermediate speed since $\left|\frac{dI}{dt}\right| = O(\varepsilon)$.

The fast equilibrium manifold

The fast equilibrium manifold is obtained by equating the right hand of (23) to zero. Solving the resulting equation for I in terms of G, we arrive at the following equation.

$$I = \frac{(R_0 - E_{G0}G)(a_0G^2 + b_0G + \mu)}{S_I G} \tag{30}$$

We observe that, on this manifold, $I \to -\infty$ as $G \to \infty$, $I \to \infty$ as $G \to 0$, and $I = 0$ at $G = \frac{R_0}{E_{G0}}$. Moreover, since (30) does not involve β_f , this surface will be parallel to the β_f - axis.

Differentiating I with respect to G gives

$$\frac{dI}{dG} = \frac{(a_0R_0 - E_{G0}b_0)G^2 - 2a_0E_{G0}G^3 - R_0\mu}{S_I G^2} \tag{31}$$

Letting

$$B = -\frac{a_0R_0 - E_{G0}b_0}{2a_0E_{G0}} \quad \text{and} \quad D = \frac{R_0\mu}{2a_0E_{G0}} \tag{32}$$

we can thus prove the following result.

Lemma 2 The curve resulting from the intersection between the fast manifold $\dot{G} = 0$ and the slow manifold $\dot{\beta}_f = 0$ has 2 relative extrema at $G = G_{M1} > 0$ and $G = G_{M2} > G_{M1} > 0$ provided (11) holds,

$$a_0R_0 - E_{G0}b_0 > 0 \tag{33}$$

and

$$D < -\frac{4}{27}B^3 \tag{34}$$

Proof

From the derivative found in (31), we get that the relative extrema will occur on the curve if the numerator of (31) vanishes, that is

$$(a_0R_0 - E_{G0}b_0)G^2 - 2a_0E_{G0}G^3 - R_0\mu = 0 \tag{35}$$

By (33), we have $B < 0$ and $D > 0$, while the discriminant of (35) is

$$\partial = -4B^3D - 27D^2$$

which is positive since (34) holds. Therefore, we can conclude that (35) has 2 positive solutions by the Descartes' Rule of Signs. This means that there exist 2 relative extrema, $G = G_{M1}$ and $G = G_{M2}$, on this curve with $G_{M1,2}$ positive. □

Let the two relative extrema on this curve on the fast manifold be denoted by $(G_{M1}, I_{M1}, \beta_{fM1})$ and $(G_{M2}, I_{M2}, \beta_{fM2})$ where

$$I_{M1,2} = \frac{(R_0 - E_{G0}G_{M1,2})(a_0G_{M1,2}^2 + b_0G_{M1,2} + \mu)}{S_I G_{M1,2}} \tag{36}$$

We note that, by (35), $G_{M1,2}$ satisfy the equation

$$G_{M1,2}^3 - \frac{R_0}{2E_{G0}}G_{M1,2}^2 + \frac{R_0\mu}{2a_0E_{G0}} = 0$$

Thus,

$$R_0 - E_{G0}G_{M1,2} = E_{G0}G_{M1,2} + \frac{R_0\mu}{a_0G_{M1,2}^2} > 0$$

By (36), we then see that $I_{M1,2} > 0$, which means both relative extrema are located in the first octant of the (G, I, β_f, I_{RP})-space in which all state variables are positive. The graph of this surface, for appropriate parametric values, may be depicted as in Fig. 1c). If we start at a point to the above and to the right of the fast manifold, according to (23), $\frac{dG}{dt} < 0$ here, then the transition will take us in the direction of decreasing G. On the other hand, starting from the area below and to the left of the fast manifold, we will be in the region where $\frac{dG}{dt} > 0$ and hence the transitions will be in the direction of increasing G. Thus, as indicated in Fig.1c), we see that the fast manifold has two stable branches, namely the portion of the surface where $G < G_{M1}$ and the one where $G_{M2} < G$. It has one unstable branch where $G_{M1} < G < G_{M2}$.

3.2 Geometric Singular Perturbation Analysis

We now let $I_{1,2}$ be the values of I on the intersection curve between the intermediate and slow manifolds at the points where $G = G_{M1,2}$, that is

$$I_{1,2} = \frac{\sigma\beta_{f1}\big(G_{M1,2}\big)\big(G_{M1,2}\big)^{\nu_h}}{k\alpha + k\big(G_{M1,2}\big)^{\nu_h}} \tag{37}$$

with

$$\beta_{f1} = \frac{r_1 G_{M1} - r_0}{r_2 G_{M1}^2} \tag{38}$$

and also let $S(G_S, I_S, \beta_{f,S})$ be the critical point where the 3 manifolds intersect, under appropriate parametric values, where

$$f(G_S, I_S) = g(G_S, I_S, \beta_{f,S}) = h(G_S, \beta_{f,S})$$

The following theorem can then be stated.

Theorem 1 The model system (23)-(25) admits a periodic solution in the form of a limit cycle surrounding the equilibrium point $S(G_S, I_S, \beta_{f,S})$, at which the 3 manifolds intersect, provided (11), (33), (34) hold, and

$$G_{M0} > \underline{G} \tag{39}$$

$$I_1 < I_{M1}, \quad I_{M2} < I_2 \tag{40}$$

where $G = G_{M0}$ is the smallest root of the following equation:

$$I_{M2} = \frac{(R_0 - E_{G0}G)(a_0G^2 + b_0G + \mu)}{S_I G}$$

Proof

The inequality (40) insures that the graph of the fast manifold where $f = 0$, for all β_f , will have, as depicted in Fig.1c), two relative extrema $\big(G_{M12}, I_{M12}, \beta_{fM2}\big)$. The inequality (39), considering the definition of $\underline{G}$, insures that the value of β_f remains positive when I reaches the height I_{M2}.

The 3 equilibrium manifolds in this case are shown together in Fig.2a), where the fast manifold $f = 0$ is shown in red, the intermediate manifold is in green and the slow manifold is in blue. The transitiontions are traced in purple, where the fast transitions are indicated by triple arrows, double arrows indicate ones with intermediate speed, and a single arrow indicates a slow transition.

We see clearly in this figure that if inequality (40) holds, then the green curve where the fast and intermediate manifolds intersect, along which $f = g = 0$, lies in the region where the manifold $f = 0$ is unstable for all G in an open interval $\Omega_S = \big(G_S - \omega, G_S + \omega\big)$ for some $\omega > 0$. $I_1 < I_{M1}$ means the intermediate manifold lies below the fast manifold for G in the interval $\big(G_S - \omega, G_S\big)$, whereas $I_{M2} < I_2$ means the intermediate manifold lies above the fast manifold for G in the interval $\big(G_S, G_S + \omega\big)$. Thus, the curve $f = g = 0$ lies in the region where the fast manifold is stable for G in Ω_S .

Starting from a generic initial point marked with A in Fig.2a), $A\big(G_0, I_0, \beta_{f,0}\big) \in \mathcal{B}$, such that $G_0 \in \Omega_s, \quad G_0 > G_S, \quad \beta_f > \beta_{f,S}$, since $\frac{dG}{dt} < 0$ here, a fast transition will develop, in the direction of decreasing G, toward the point B on the nearest stable branch of the manifold $f = 0$, while I and β_f remain frozen. The transition is made at a fast speed relatively because $\left|\frac{dG}{dt}\right| = O(1)$.

Once B is reached, the intermediate system has become active. Here, we are below the intermediate manifold so that $\frac{dI}{dt} > 0$ and a transition is made, in the direction of increasing I at an intermediate speed, since $\left|\frac{dI}{dt}\right| = O(\varepsilon)$, until the point C is reached, where the stability is lost, and a quick jump brings the system to the other stable branch of the manifold $f = 0$ at point D. Here, $\frac{dI}{dt} > 0$ and so a motion at intermediate speed develops down the surface $f = 0$ until the point E is reached where the stability of the manifold is again lost and a quick jump brings the trajectory to the point F on other stable branch. Next, for the same reason as before, a transition of intermediate speed develops on this manifold in the direction of increasing I again to H just missing the point C since β_f has been slowly decreasing. The cycling motion repeats while β_f decreases slowly, as

$\left|\frac{d\beta_f}{dt}\right| = O(\varepsilon, \delta)$, until the manifold $f = h = 0$ is reached at a point J. A quick jump to K is followed by a upward transition to L where the stability is lost. A quick jump is then made to M followed by a downward transition at intermediate speed back to J thereby completing a stable limit cycle $JKLMJ$ surrounding the unstable steady state $S(G_S, I_S, \beta_{f,S})$.□

Of equal interest, is the case in which the system is stable and the state variables all tend towards their respective steady state values. By similar arguments, we can prove the following result.

Theorem 2 The model system (23)-(25) admits an equilibrium solution, $(G_S, I_S, \beta_{f,S})$, which is locally asymptotically stable provided (11), (32), (34) and (39) hold, and the inequalities in either Case 1 or Case 2 below are satisfied.

Case 1: $I_1 > I_{M1}$, and $I_2 > I_{M2}$ (41)

Case 2: $I_1 < I_{M1}$, and $I_2 < I_{M2}$ (42)

Proof

The arguments for Case 1 or Case 2 are essentially the same. We will therefore only show Case 2 here. In this case, the shapes and positions of the 3 equilibrium manifolds are as depicted in Fig.2b), for appropriate parametric values. The inequalities in (42) insure that a portion of the curve $f = g = 0$ intersects the curve $f = h = 0$ at the point $S(G_S, I_S, \beta_{f,S})$ that is located on a stable portion of the fast manifold.

Again, Starting from a generic initial point marked with A in Fig.2b), $A(G_0, I_0, \beta_{f,0}) \in \mathcal{B}$, such that $G_0 \in \Omega_s$, where, say $G_0 < G_S, \beta_f > \beta_{f,S}$ since $\frac{dG}{dt} > 0$ here, a fast transition will develop, in the direction of increasing G, toward the point B on the nearest stable branch of the fast manifold $f = 0$, while, for the time being, I and β_f remain frozen.

Once B is reached, the intermediate system has become active. Here, $\frac{dI}{dt} < 0$ and a transition is made at intermediate speed in the direction of decreasing I, until the point C is reached, where the stability is lost. As before, a quick jump brings the system to the other stable branch of the manifold $f = 0$ at point D.

Here, $\frac{dI}{dt} > 0$ and so a motion at intermediate speed develops upward along the surface $f = 0$ until we arrive at the point E on the curve where the intermediate manifold intersects the fast manifold and the intermediate dynamic now becomes active. Since this is still on the stable portion of the fast manifold, stability is maintained and a transition is then made slowly along this curve in the direction of increasing β_f, since $\frac{d\beta_f}{dt} > 0$ here. Eventually, the point where the curve $f = g = 0$ intersects the slow manifold so that the 3 manifolds intersect at the point $(G_S, I_S, \beta_{f,s})$ is reached, marked by S in Fig.2b), where transitions stop since $\frac{dG}{dt} = \frac{dI}{dt} = \frac{d\beta_f}{dt} = 0$ here. Thus, this is the case where the steady state is locally asymptotically stable. □

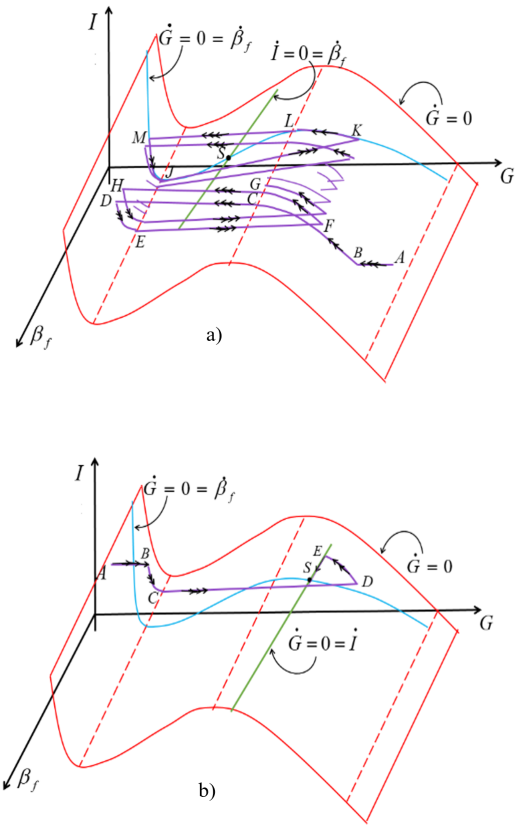

Figure 2: The fast (red), intermediate (green) and slow (blue) manifolds are here shown in the 3-dimensional space with transitions of fast speed (triple arrows), intermediate speed (double arrows) and slow speed (single arrow) in the case that a) the model system admits a limit cycle surrounding the steady state S, described in Theorem 1, and b) the trajectory tends to a stable steady state in case 2 of Theorem 2

In the next section, we show numerical simulations of the model under investigation to support our theoretical predictions.

4 Model Simulation

We present here numerical simulations of the model system (23) - (26) in various cases mentioned above. The values of those parameters not involved in the satisfaction of conditions that delineate different dynamic behaviors are estimated or based on those utilized in the literatures, mainly in [6],[7], and [15]. The

units of the variables have already been scaled out by the introduction of new variables and parameters in (15) - (22). Thus, what units the parameters have depends on the units with which you choose to measure the state variables, ensuring that both sides of Equations (23) - (26) have the same units. To specify physiological values for the model parameters, we rely as much as possible on [6] and [7], where rigorous review of the literature was carried out to identify physiological values for the relevant parameters in their model. Since information for some parameters is limited, most were based on empirical observations and their values were derived using well established statistical methodologies [7]. Some of the parameters are here varied to satisfy the inequalities required for each of the cases to hold. The variations reflect various symptoms of the patients which will be explained accordingly.

It must be mentioned here that, according to Viceconti et al. [21], the utilization of integrative approaches to biomedical research creates the need to manage large amounts of data that are radically heterogeneous in structure, complicated by the fact that more often than not these data are measured or observed at very different dimensional and/or temporal scales. Their study in [21] describes a first attempt at providing a strategical environment for homogeneous biomedical data defined over radically different spatial or temporal scales. New strategies for the management are currently discovered and developed for the management of temporal multi-scaling or highly heterogenous data types. It is, however, beyond the scope of our research.

The model system (23) - (26) is simulated with parametric values satisfying inequalities identified in Theorem 1, in which case the model system is predicted to admit limit cycles towards which the solution trajectory tends as time progresses, as seen in Fig.3. The corresponding time series of the 4 state variables are shown in Fig.4, exhibiting sustained oscillation mimicking clinical data reported in several literatures.

Here, $G_0 = 2, I_0 = 2, \beta_{f0} = 3, I_{RP0} = 1,$
$t_0 = 0, R_0 = 1.12, S_I = 0.889, E_{G0} = 0.054,$
$a_0 = 1, b_0 = 0.2347, c_0 = 0.000313, i = 0.000187,$
$\sigma = 0.20592, \alpha = 0.0017, k = 6.5, r_0 = 0.00001,$
$r_1 = 0.0884, r_2 = 0.024, k_D = 0.001,$
$k_{SARS} = 0.15, k_{ACE2} = 0.4, k_{ACE2,0} = 0.385,$
$D_S = 0.0372, k_G = 0.1, k_{eff} = 0.689, \Delta = 1,$
$\varepsilon = 0.001, \delta = 0.8$.

The inflammatory response I_{RP} also oscillates as time passes. This reflects a control system which is working comparatively efficiently, in which an increase in the glucose level triggers the beta cells to become functional and secrete insulin in response. The rise in insulin is then followed by the satisfactory drop in the glucose level. It is then no longer necessary for the beta cells to produce the hormone insulin, the level of which then drops with a little time lag following the glucose drop.

The numerical solution of (23) - (26) in Case 2, where inequalities identified in Case 2 of Theorem 2 are satisfied, is shown in Fig.5 and 6. Case 1 is similar, so that the simulation has been omitted.

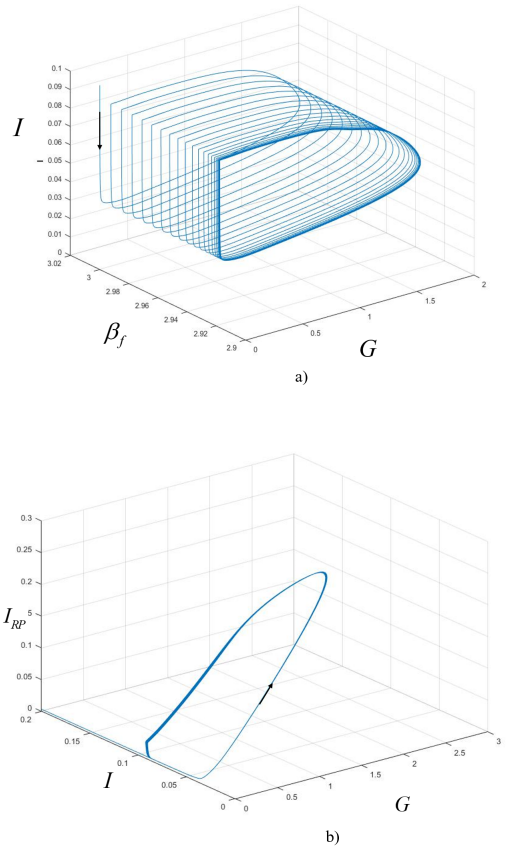

Figure 3: Numerical solution of (23) - (26) in the case that the inequalities in Theorem 1 are satisfied. The solution trajectory is seen here to tend towards the stable limit cycle as time passes as theoretically predicted.

Here, $G_0 = 0.1, I_0 = 0.1, \beta_{f0} = 0.1,$
$I_{RP0} = 0.2, t_0 = 0, R_0 = 1.6, E_{G0} = 0.8,$
$S_I = 0.04998, a_0 = 1, b_0 = 0.00001,$
$c_0 = 0.000413, i = 0.000087, \sigma = 0.00352, \alpha = 2,$
$k = 11, r_0 = 0.001, r_1 = 0.0884, r_2 = 0.074,$
$k_{SARS} = 0.15, k_{ACE2} = 0.4, k_{ACE2,0} = 0.385,$
$k_D = 0.001, D_S = 0.0372, k_G = 0.1,$
$k_{eff} = 0.689, \Delta = 1, \varepsilon = 0.31, \delta = 0.28.$

We can observe clearly here that there is a definite delay after the level of glucose in the bloodstream increases before insulin is secreted in response. The difference from the previous case where sustained oscillation is exhibited is that the value of R_0 is larger,

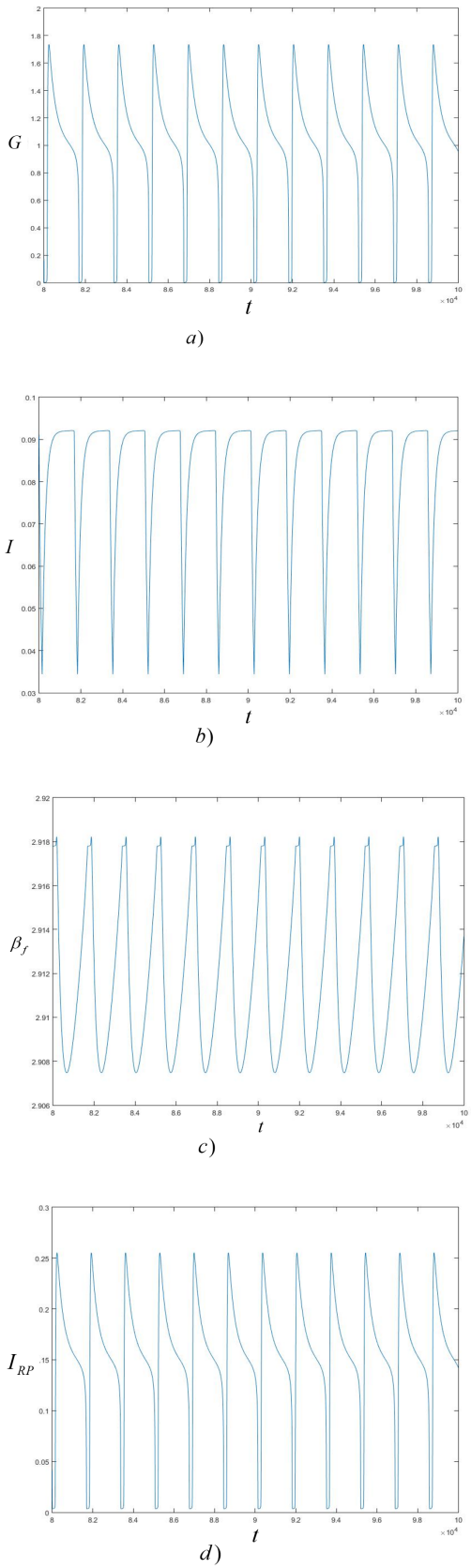

Figure 4: The time courses of a) glucose concentration, b) insulin concentration, c) functional beta cells, and d) the inflammatory response, in the case shown in Fig.3. All 4 state variables are seen to oscillate periodically as time progresses.

which drives glucose to increase more quickly, while a smaller S_I has the effect of slowing down the response of insulin. Moreover, σ is very much smaller which means the increase in G is felt to a lesser degree by the rate of insulin production, so that it can manage to bring down the glucose level only a little before it settles to a rather high steady state level. More importantly, we see that the inflammatory response is able to rise up to a sustainably high level, which is not desirable in the clinical point of view of a patient with comorbidity with COVID-19.

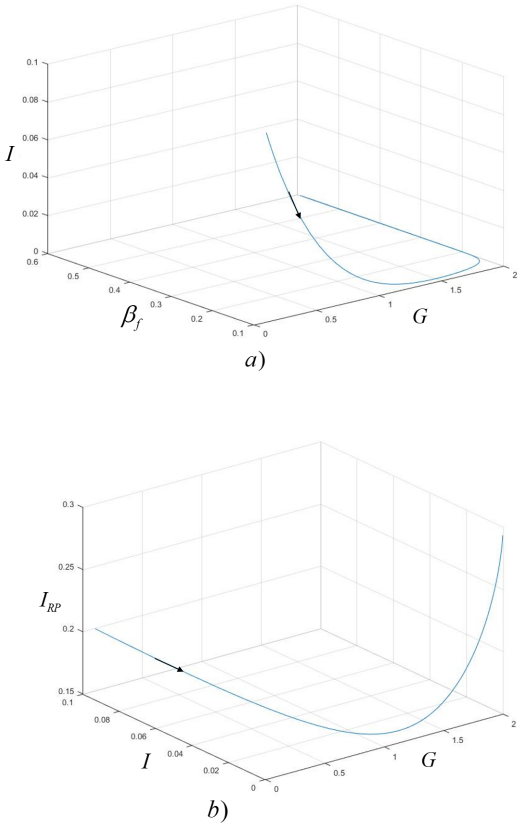

Figure 5: Numerical solution of (23) - (26) in the case that the inequalities in Theorem 2 are satisfied. The solution trajectory is seen here to tend towards the locally asymptotically stable steady state as time passes as theoretically predicted.

5 Discussion and Interpretation

Considering the conditions (34) and (39) in both Theorem 1 and Theorem 2 which ensure that the solutions remain bounded and local stability is maintained, we see that we must have

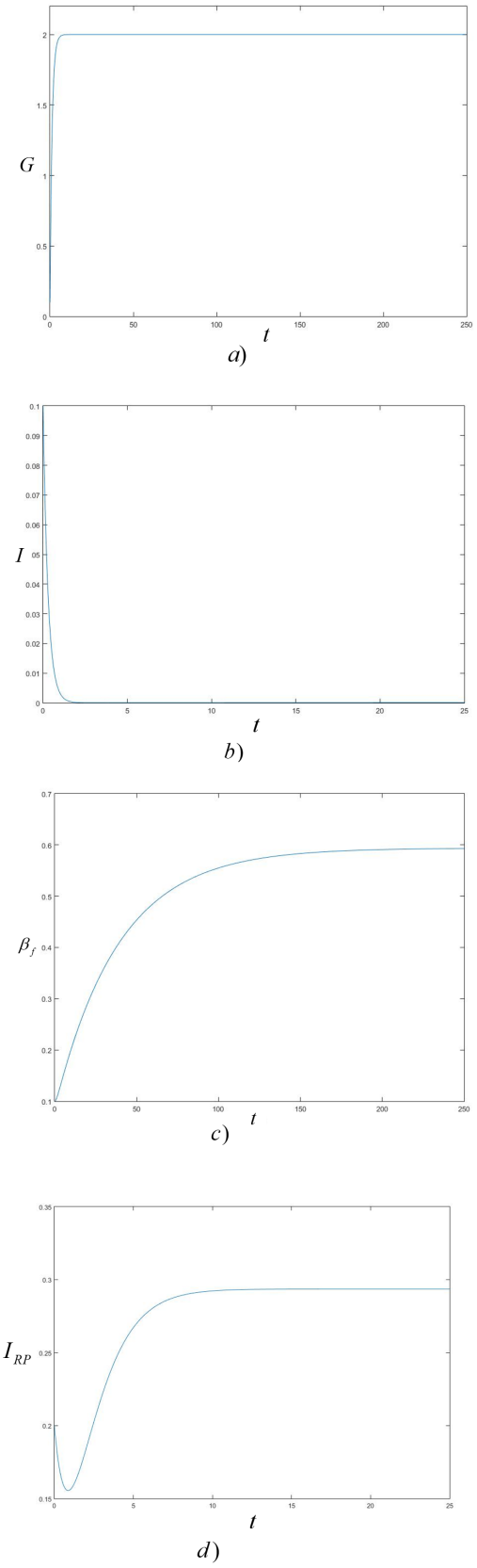

Figure 6: The time courses of a) glucose concentration, b) insulin concentration, c) functional beta cells, d) and the inflammatory response, in the case shown in Fig.5. All 4 state variables are seen to tend toward their respective steady state values as time progresses.

$$\mu < \frac{a_0 R_0^2}{27 E_{G0}^2} \tag{43}$$

for (34) to hold, and

$$r_0 < r_1 G_{M0} \tag{44}$$

for (39) to hold. Inequality (43) will be satisfied if μ , the sum of c_0 and i, should be sufficiently small so that it is smaller than the quantity on the right of the inequality (43). This means that the zero glucose coefficient in the numerator of the last term in (23), reflecting insulin resistance, is sufficiently small. Essentially, insulin resistance should be sufficiently small when negligible glucose is present.

In addition, r_0 , the death rate of β-cells at zero glucose, must be small in comparison to r_1, the first order coefficient for β-cells replication. This means β-cells should be slow in dying and, at the same time, they should be able to replicate quickly even with low glucose activation. If the above conditions are not met, the system should be recognized as defective. Abnormal dynamics could be expected if these 2 conditions are violated. Moreover, considering the position of the slow manifold given by (28) relative to the fast and intermediate manifolds in the phase space, we can see that trajectories, traced by the singular perturbation arguments, will develop in a way that is indicative of symptoms of serious insulin resistance if

$$\begin{aligned} \beta_f\Big|_{g=0} &= \frac{I(\hat{G})\left(k\alpha + k\hat{G}^{\nu_h}\right)}{\sigma \hat{G}^{\nu_h}} \\ &> \frac{r_1 \hat{G} - r_0}{r_2 \hat{G}^2} = \beta_f\Big|_{h=0} \end{aligned} \tag{45}$$

which reflects a disfunctional control system since it appears not to be able to produce insulin, or activate the β-cells to do so to decrease the glucose level in the bloodstream. Condition (45) can be achieved if k is sufficiently large or σ is sufficiently small, in which case $k \gg 1$ or $\sigma \ll 1$ insulin is not secreted sufficiently in response to high glucose and consequently, insulin level continues to drop necessitating exogenous insulin supplements to bring the system under control. We show a simulated time series of the model's solution in this scenario in Fig.7 with $G_0 = 0.8, I_0 = 0.5, \beta_{f0} = 0.01, I_{RPO} = 2, t_0 = 0, R_0 = 2, E_{G0} = 0.06, S_I = 0.01, a_0 = 1, b_0 = 0.00001, c_0 = 0.000313, i = 0.000187, \sigma = 0.009, \alpha = 0.07, k = 8, r_0 = 0.007, r_1 = 0.018, r_2 = 0.074, k_{SARS} = 0.15, k_{ACE2} = 0.4, k_{ACE2,0} = 0.385, k_D = 0.001, D_s = 0.0372, k_G = 0.1, k_{ff} = 0.689, \delta = 1, \varepsilon = 0.21, \delta = 0.28$.

Considering (26), the presence of high ACE2 inhibitor can contribute to high rate of inflammatory

response increase. ACE inhibitors are a class of drug known to cause inflammation and allergic reactions [23]. Fine tuning of the drug therapy may be a good strategy to compensate for worrisome constant inflammatory activation, in the case where the rise of glucose level is unchecked and insulin level is persistently low.

Although inflammation is beneficial, since it protects against infection and injury, when that response is constantly triggered, it can be harmful the body instead of healing it in the long run. As reported in [24], the prolonged inflammatory activation and subsequent response commonly result in increased susceptibility to coronavirus infection leading to more severe respiratory failure and end-organ damage in patients with SARS-CoV-2.

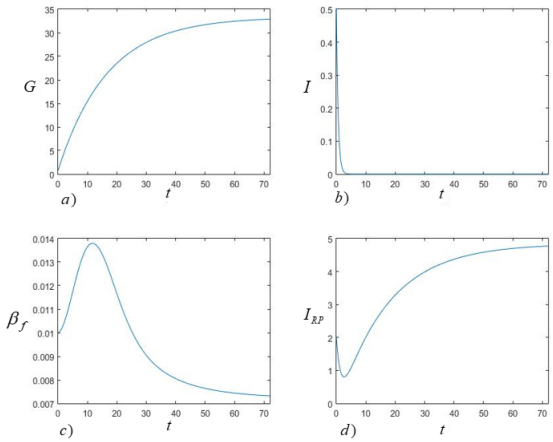

Figure 7: The time courses of (a) glucose concentration, (b) insulin concentration, (c) functional beta cells, and (d) the inflammatory response, in the scenario in which the glucose level quickly rises while insulin drops and the inflammatory response rises to a high level.

6 Conclusion

A model of insulin-glucose control system, incorporating inflammatory response, which, when triggered constantly, over time, can harm the body instead of healing it, has been studied. The inflammatory activation and subsequent response, may more commonly than not lead to increased susceptibility to coronavirus infection. Theoretical analysis by the geometrical singular perturbation technique, well suited for such systems subject to highly diversified time scales, has been carried out, and numerical simulations discussed in terms of the delineating conditions on the system's parameters. The state variables tracked by our model, the glucose and insulin concentrations, the functional β cells and the inflammatory response will eventually tend asymptotically to their corresponding steady state values, or oscillate in a bounded fashion, provided that the zero glucose coefficient in the numerator of the last term which represents insulin resistance, in the rate equation for glucose level, is sufficiently small. Essentially, insulin resistance should be sufficiently small when negligible glucose is present.

The conditions that are indicative of a dysfunctional system, appearing not to be able to produce insulin, or activate the β-cells to do so to decrease the glucose level in the bloodstream, are manifested if k is too large or σ is too small, in which case $k \gg 1$ or $\sigma \ll 1$. Insulin is not secreted sufficiently in response to high glucose and consequently, insulin level continues to drop necessitating exogenous insulin supplements to bring the system under control.

Further research could involve investigating the impacts of food intakes and exercises, as well as temporal drug administrations and periodic hormone supplements, which can be incorporated in to the model derived here with relative ease. Such studies can lead to additional insights and valuable suggestions of efficient treatment protocols for patients who could be exhibiting various symptoms of comorbidity.

Acknowledgment. This research has received funding support from the NSRF via the Program Management Unit for Human Resource & Institutional Development, Research and Innovation (grant number B05F640231). Also, this research is partially supported by the Centre of Excellence in Mathematics, Ministry of Higher Education, Science, Research and Innovation, Thailand(grant number RG-01-65-01-1).

References:

[1] S. Babashov, Predicting the Dynamics of Covid-19 Propagation in Azerbaijan based on Time Series Models,*WSEAS TRANSACTIONS on ENVIRONMENT and DEVELOPMENT*, DOI: 10.37394/232015.2022.18.99

[2] G. Makanda, A mathematical model for the prediction of the impact of coronavirus (COVID-19) and social distancing effect, *WSEAS TRANSACTIONS on SYSTEMS and CONTROL*, DOI: 10.37394/23203.2020.15.60

[3] Y. Riyani, S. Andriana, K. Mardiah, L. Suherma, B. Riyadhi, A. Arianto, K. Khamimi, J. Jakfar, E. Endri, Stock Market Reactions before and during the COVID-19 Pandemic: Evidence from Indonesia, *WSEAS TRANSACTIONS on BUSINESS and ECONOMICS* DOI: 10.37394/23207.2022.19.104

[4] C. Smith, A dangerous new coronavirus complication was discovered - and it never goes away if you get it.(accessed: 06.03.2022), *https://bgr.com/science/coronavirus-symptoms-complications-diabetes-onset-after-covid-19/*.

[5] D. Campbell, Covidl19: people with type 1 diabetes more likely to die than those with type 2 l study, Diabetes (accessed: 06.03.2022) ,*https://www.theguardian.com/society/2020/may/20/type-1-diabetics-type-2-coronavirus-nhs-study*

[6] A. De Gaetano, T. Hardy, B. Beck, E. Abu-Raddad, P. Palumbo,J.B. Valleskey, N. Pϕrksen, Mathematical models of diabetes progression. *Am J Physiol Endocrinol Metab*. 2008 Dec;295(6):E1462-79. doi: 10.1152/ajpendo.90444.2008.

[7] P. Barbiero , P. Li ó,The Computational Patient has Diabetes and A COVID, medRxiv (accessed: 06.03.2022),*https://doi.org/10.1101/2020.06.10.20127183.*

[8] Y. Lenbury, S. Ruktamatakul, S. Amornsamarnkul, Modeling insulin kinetics: responses to a single oral glucose administration or ambulatory-fed conditions. *Biosystems*. 2001 Jan;59(1):15-25.

[9] D.V. Giang, Y. Lenbury, A. De Gaetano, Delay model of glucose-insulin systems: Global stability and oscillated solutions conditional on delays, *Journal of Mathematical Analysis and Applications*, Volume 343, Issue 2, 2008, Pages 996-1006.

[10] P. Palumbo and S. Panunzi and A. De Gaetano, Qualitative behavior of a family of delay-differential models of the Glucose-Insulin system. *Discrete and Continuous Dynamical Systems. Series B*. No.7, 2007, 399-424.

[11] L. Kardar , A. Fallah , S. Gharibzadeh , F. Moztarzadeh, Application of fuzzy logic controller for intensive insulin therapy in type 1 diabetic mellitus patients by subcutaneous route. *WSEAS Transactions on Systems and Control*, Vol 3, No. 9, 2008, 712-721.

[12] M. Chuedoung , W. Sarika , Y. Lenbury, Dynamical analysis of a nonlinear model for glucose-insulin system incorporating delays and b-cells compartment. *Nonlinear Analysis - theory Methods & Applications - NONLINEAR ANAL-THEOR METH APP*. Vol.71, No. 12, 2009, e1048-e1058.

[13] X. Cao, D. Liu, S. Yu Wang.,Mathematical Modelling and Stability Analysis for Diabetes Predicting System ,*WSEAS Transaction on Mathematics*, Vol.14, 178-191, 2015.

[14] A. Felman, What to know about insulin resistance. MedicalNewsToday, medically reviewed by Deborah Weatherspoon on March 26, 2019,*https://www.medicalnewstoday.com/articles/305567.php*.

[15] C. Ratanakul, Y. Lenbury, J. Suksamran, Singular Perturbation Analysis for Identification of Dynamic Behaviour and Stability of a Nonlinear Model of Long Term Progression of Diabetes Mellitus. *WSEAS Transactions on Mathematics*,2020, 523-530.

[16] Mechanism Of Action Of Insulin On Blood Glucose Level, Diabetes Talk,https://diabetestalk.net/insulin/mechanism-of-action-of-insulin-on-blood-glucose-evel♯:∼:text=Insulin%20has%20a%20number%20of%20actions%20on%20the,the%20cells%20by%20activating %20the%20sodium-potassium%20cellular%20channels

[17] K. Romito, A. Husney, T. O'Young, D. C.W. Lau, Learning About ACE Inhibitors and ARBs for Diabetes, available from: https://healthy.kaiserpermanente.org/health-wellness/health-encyclopedia/he.learning-about-ace-inhibitors-and-arbs-for-iabetes.abq4936♯:∼:text=When%20you%20have%20diabetes%2C%20taking%20an%20ACE%20inhibitor, High%20blood%20pressure%20can%20damage%20the%20kidneys%2C%20too.

[18] Art 5(3) - Sotrovimab (VIR-7831 - GSK4182136) for the treatment of COVID-19 (GSK) - assessment report, European Medicines Agency, 20 May 2021

[19] S. Muratori, S. Rinaldi.,Low- and high- frequency oscillations in three-dimensional food chain systems. ,*SIAM Journal of Applied Mathematics*, Vol.52,1992,1688-1706.

[20] S. Rinaldi, M. Scheffer, Geometric Analysis of Ecological Models with Slow and Fast Processes. *Ecosystems 3*, 2000, 507□521.

[21] M. Viceconti, G. Clapworthy, D.Testi, F.Taddei, N.McFarlane, Multimodal fusion of biomedical data at different temporal and dimensional scales, *Computer Methods and Programs in Biomedicine*, Vol. 102,

Issue 3, June 2011, Pages 227-237, https://doi.org/10.1016/j.cmpb.2010.04.017)

[22] K. Hobson,Is Inflammation Bad for You or Good for You? Health News from NPR,*https://www.npr.org/sections/health-shots/2017/07/21/538377221/is-inflammation-bad-for-you-or-good-for-you*,2017.

[23] T. Eyre and V. Van-Hamel-Parsons and L. Mun Wang and K. A. Hughes and Timothy J Littlewood, An unusual cause of anaemia of chronic disease: lisinopril-induced chronic inflammatory state.*PubMed*, 2011, doi: 10.1155/2011/939080.

[24] R. M. Inciardi, S. D. Solomon, P. M. Ridker, M. Metra, Coronavirus 2019 Disease (COVID-19), Systemic Inflammation, and Cardiovascular Disease. *Journal of the American Heart Association*, 2020.

Contribution of individual authors to the creation of a scientific article (ghostwriting policy)

Chontita Rattanakul carried out parts of the analysis, checked all proofs and carried out model simulations and figures production.
Yongwimon Lenbury constructed the model equations in the form that singular perturbation analysis could be consequently carried out, and provided the drawings and arguments concerning the geometric singular perturbation.
Nathnarong Khajohnsaksumeth created the computer codes for the simulations and production of the manuscript.
Charin Modchang provided the initial fundamental understandings of the problem of interest, specifically the mechanisms related to comorbidity between diabetes and COVID-19, which assisted in the model formulation.

Sources of funding for research presented in a scientific article or scientific article itself

This research has received funding support from the NSRF via the Program Management Unit for Human Resource & Institutional Development, Research and Innovation (grant number B05F640231). Also, this research is partially supported by the Centre of Excellence in Mathematics, Ministry of Higher Education, Science, Research and Innovation, Thailand (grant number RG-01-65-01-1).

Creative Commons Attribution License 4.0 (Attribution 4.0 International , CC BY 4.0)